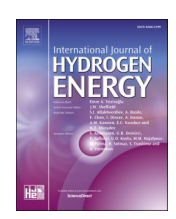
ELSEVIER

Contents lists available at ScienceDirect

# International Journal of Hydrogen Energy

journal homepage: www.elsevier.com/locate/he



# Check for updates

# Predicting NOx emissions from ammonia engines – Fuel and thermal effects

A. Cova-Bonillo <sup>a</sup>, P. Gabana <sup>b</sup>, N. Khedkar <sup>a</sup>, G. Brinklow <sup>a</sup>, M. Wu <sup>a</sup>, J.M. Herreros <sup>a</sup>, S. Zeraati-Rezaei <sup>a</sup>, A. Tsolakis <sup>a,\*</sup>, A. Ambalakatte <sup>c</sup>, A. Cairns <sup>c</sup>, J. Hall <sup>d</sup>

- <sup>a</sup> Department of Mechanical Engineering, University of Birmingham, Edgbaston, B15 2TT, UK
- <sup>b</sup> Department of Energy and Fluid Mechanics Engineering, University of Valladolid, E-47011, Valladolid, Spain
- <sup>c</sup> Powertrain Research Centre, University of Nottingham, Nottingham, NG7 2RD, UK
- <sup>d</sup> MAHLE Powertrain Limited, Costin House, St., James Mill Road, Northampton, NN5 5TZ, UK

#### ARTICLE INFO

Handling Editor: Ramazan Solmaz

Keywords:
Ammonia
NOx
Prediction
Combustion
Engine
Kinetic mechanism

#### ABSTRACT

Ammonia, a promising zero-carbon fuel, faces engine application challenges from high NOx and ammonia slip. A key knowledge gap remains in predicting NOx and ammonia slip with chemical kinetic mechanisms within complex engine environments, beyond simple metrics. This research evaluates 14 ammonia combustion mechanisms in a spark-ignition (SI) engine model, using a two-zone thermodynamic approach. Experimental data from stoichiometric pure ammonia combustion in a research engine validate NOx predictions. The analysis details NOx formation, NH $_3$  slip, NO production rates, and differentiates thermal-NOx from fuel-NOx. While most mechanisms predict NOx within 20 % error, those by Otomo, Stagni, and Nakamura show superior accuracy. Furthermore, a significant divergence in N $_2$ O predictions was found; only the Konnov mechanism yielded plausible concentrations (14–24 ppm), exposing a common limitation in other models. This study identifies thermal-NOx as ~75 % of total NOx, offering vital insights for targeted emission control and guiding mechanism selection for engine development.

#### 1. Introduction

The transportation sector is a major global contributor to greenhouse gas emissions, responsible for approximately 15 % of the anthropogenic total, necessitating comprehensive mitigation strategies [1]. This challenge is particularly acute in nations, where transportation has overtaken the power sector as the primary source of emissions [2]. Ammonia has emerged as a promising carbon-free fuel, primarily due to its high capacity as hydrogen carrier. Compared to molecular hydrogen, it offers clear advantages in terms of storage and transportation logistics [3], while also exhibiting a notably higher volumetric energy density [4]. Beyond these practical benefits, its potential for sustainable production is gaining traction through the advancement of green synthesis pathways powered by renewable energy sources [5]. These innovations present a feasible alternative to the traditional Haber–Bosch process [6]. However, significant combustion challenges remain, including its low flame speed and high autoignition temperature [7]. This high resistance to auto-ignition, in particular, has historically posed a challenge for engine applications; for instance, achieving compression-ignition with pure ammonia was shown to require extremely high compression ratios (exceeding 30:1) [8]. A further challenge lies in managing the emissions from ammonia combustion, which are a concern across practical applications [9]. This includes the potential for increased NO<sub>x</sub> emissions, particularly when ammonia is used in power system [10], as well as N<sub>2</sub>O, a critical greenhouse gas due to its high warming potential [11]. A detailed understanding of the ammonia combustion process is essential to overcome such challenges. While some practical applications may use combustion enhancers like hydrogen [12], a foundational understanding of pure ammonia chemistry is a critical prerequisite. This study therefore focuses on establishing a validated baseline for pure ammonia, providing a robust platform for future investigations into more complex fuel blends. Combustion modelling is critical for understanding reaction processes, designing experiments, and predicting emissions. Numerous chemical kinetic mechanisms (CKMs) have been developed in recent years to model ammonia combustion under various conditions accurately. These advancements have enabled increasingly accurate predictions of key indicators such as ignition delay, flame speed, and emissions. These mechanisms vary in complexity and range of applications, with a trade-off between computational affordability and accuracy tending to be the criterion for their purpose. Alnasif et al. [13]

E-mail address: a.tsolakis@bham.ac.uk (A. Tsolakis).

<sup>\*</sup> Corresponding author.

emphasized that while significant strides have been made in ammonia combustion modelling over the past 50 years, challenges persist, particularly in predicting NOx emissions and extending the applicability of mechanisms across broader air-fuel ratios. It is common practice to evaluate different CKMs to compare their performance and suitability for specific applications; this comparative approach has been rigorously applied to foundational fuels like hydrogen [14] and syngas [15].

Kawka et al. [16] studied eight published mechanisms (Mével 2009 [17], Klippenstein\_ 2011 [18], Abian\_2015, Zhang\_2017 [19], Glarborg\_2018 [20], Shrestha\_2018 [21], Song\_2019 [22], and Kovács\_2020 [23]) for homogeneous ammonia combustion using experimental data from shock tubes and flow reactors. The Glarborg\_2018 and Shrestha\_2018 mechanisms performed well in predicting ignition delay times, but none of the mechanisms accurately reproduced NO, N2O, and NH3 concentration profiles in flow reactors. In a subsequent study, Alnasif et al. [24] investigated NO formation/consumption in NH<sub>3</sub>/H<sub>2</sub> mixtures using premixed stabilized stagnation flames, comparing 67 CKMs against experimental measurements. Glarborg and Nakamura's mechanisms showed strong predictive capabilities under lean and stoichiometric conditions. Key reactions influencing NO formation (HNO +  $H\rightleftharpoons NO + H_2$ ,  $HNO + O\rightleftharpoons NO + OH$ , and  $NH + O\rightleftharpoons NO + H$ ) and consumption  $(NH_2+NO\rightleftharpoons N_2+H_2O, NH_2+NO\rightleftharpoons NNH+OH, NH+NO\rightleftharpoons N_2O)$ + H, and N + NO $\rightleftharpoons$ N<sub>2</sub>+O) were identified.

Using homogeneous adiabatic autoignition models, Rabbani et al. [25] compared five ammonia oxidation mechanisms (Glarborg\_2018 [20], Shrestha 2018 [21], Li 2019 [26], Stagni 2020 [27], Zhang 2021 [28]). Key differences were found in the duration of chemical runaways and the role of N2 chemistry, particularly reactions involving species with two nitrogen atoms. Similarities were observed in the thermal runaway, driven by OH-producing and consuming reactions, such as  $NH_2+NO \rightarrow NNH + OH$  and  $OH + H_2 \rightarrow H + H_2O$ . Nineteen CKMs for the combustion of H<sub>2</sub>/NH<sub>3</sub> mixtures under conditions commonly found in industrial combustion reactors were compared by Yuan et al. [29]. Their study highlighted significant discrepancies in the predictions of key combustion parameters, such as laminar burning velocities, ignition delay times, and species concentrations, among the different models. The authors introduced a curve-matching method to complement traditional point-wise comparisons, enabling a more nuanced assessment of model performance. This approach revealed that the accuracy of mechanism predictions can vary significantly depending on the evaluation method employed. Similar comparative studies, such as those by Girhe et al. [30], Yuan et al. [29], Xiao and Valera-Medina [31] and Zhang et al. [32] further contributed to the evaluation of kinetic mechanisms for ammonia combustion and/or NO<sub>X</sub> emissions. Furthering the complexity of ammonia combustion modelling, accurately quantifying thermal-NO<sub>X</sub> and fuel-NO<sub>X</sub> contributions in emissions remains a significant challenge. This differentiation enables targeted strategies to minimize NO<sub>X</sub> formation based on its primary source. Thermal-NO<sub>X</sub>, originating from atmospheric nitrogen oxidation via the Zeldovich mechanism [33], is relatively well-understood. However, fuel-NO<sub>X</sub>, arising from complex reactions involving nitrogen within the ammonia fuel (HNO/NH/N radicals with OH\*, O2, and O\*) [34], presents greater predictive difficulties. Researchers have employed fictitious species techniques, introducing isotopic species, to decouple these NO<sub>X</sub> sources. Yang et al. [34,35] reported that thermal and fuel NO<sub>X</sub> concentrations were of the same order of magnitude, although their relative proportions varied significantly with engine operating conditions. Wu et al. [36] found that increasing the ammonia energy contribution from 20 % to 60 % in diesel increased fuel NOx but decreased total NOx. This method, however, overestimated the total NO<sub>X</sub> because it does not consider the radical interactions between atmospheric and fuel nitrogen, resulting in higher total NOx than the original mechanism, although within the same order of magnitude.

While other foundational studies have provided valuable large-scale comparisons of kinetic mechanisms, they have focused on idealized laboratory systems. These include evaluations against data from shock

tubes and flow reactors [16], burner-stabilized stagnation flames for  $NH_3/H_2$  blends [24], and large-scale comparisons using novel evaluation methods like curve-matching [29]. However, a critical knowledge gap remains: how these mechanisms perform under the complex, transient conditions of a real internal combustion engine. This work directly addresses that gap by providing a comprehensive evaluation of 14 prominent ammonia combustion mechanisms validated against experimental data from a spark-ignition (SI) engine fueled with pure ammonia. This approach challenges the CKM predictions against a more realistic operational environment, offering a more stringent and practical assessment of the models' suitability for applied engine simulations. The findings contribute to a better understanding of NOx formation pathways to guide both the selection of appropriate models and the development of targeted emission inhibition and abatement strategies.

#### 2. Methodology

Experimental data for pure ammonia combustion is generated from a modified four-strokes single-cylinder MAHLE DI3 research engine. This research engine features an increased compression ratio (12.39), high-energy ignition system and variable valve timing to improve ammonia combustion stability, which is particularly important for extending the stable operating range towards lower loads. The experimental setup and procedures are detailed in Ambalakatte et al. [37]. Engine specifications are provided in Table 1.

Table 2 presents relevant experimental results from Ambalakatte et al. [37], that were used as the input conditions and validation targets for this simulation study. Data is shown for three engine speeds, each at four different load points, all utilizing pure ammonia as fuel under stoichiometric conditions ( $\lambda=1$ ). Spark timing (ST) was systematically adjusted to Maximum Brake Torque (MBT) with combustion phased to maintain a 50 % mass fraction burned of 8.5  $\pm$  0.5 crank angle degrees (CAD) after top dead centre (aTDC). Table 2 also includes valve timings, NOx emissions (with a reported measurement accuracy of better than  $\pm 1$  %), and unburned ammonia (NH3-slip, with a reported accuracy of  $\pm 2$  %). NOx refers to the sum of nitrogen dioxide (NO2) and nitric oxide (NO).

## 3. The investigated mechanisms

The 14 CKMs are applied to a two-zone SI engine model to analyse their NOx predictive capabilities under ammonia combustion. The selection of these mechanisms was designed to provide a broad and representative sample, based on their diversity in size and complexity, and the inclusion of both recent state-of-the-art models and established foundational mechanisms. These models, developed or updated in recent years, provide a relevant basis for evaluation, although it is acknowledged that they have specific recommendations for use which inherently limit their applicability to certain temperature ranges, equivalence ratios, and other parameters. Table 3 summarises these CKMs, including the number of species and reactions in each mechanism (NS/NR). A concise overview of the development history and key features of each mechanism is provided in Appendix A.

Table 1
Spark Ignition engine details.

Parameter	Specification
Number of cylinders	1
Number of strokes	4
Compression ratio	12.39
Engine displacement	400 cc
Bore	83.0 mm
Stroke	73.9 mm
Rated power	33.5 kW @ 6000 rpm
Connecting Rod Length	123 mm
Piston Offset	0.8 mm

**Table 2**Relevant measured operating conditions.

Condition/Tag	ST CAD (aTDC)	NIMEP bar	Torque Nm	IVO CAD	IVC CAD	EVO CAD	EVC CAD	NOx ppm	NH <sub>3</sub> slip ppm
1800 rpm/16 bar	-27	16	48	-16	204	250	22	1360	6502
1800 rpm/14 bar	-28	14	41					1338	6422
1800 rpm/12 bar	-30	12	36					1447	6718
1800 rpm/9 bar	-34	9	27					1464	8146
1400 rpm/12 bar	-27	12	35					1304	7100
1400 rpm/10 bar	-28	10	30					1350	6774
1400 rpm/9 bar	-31	9	26					1377	7191
1400 rpm/8 bar	-33	8	24					1641	7984
1000 rpm/12 bar	-21	12	37	-9	211	243	15	1263	6539
1000 rpm/10 bar	-24	10	30					1270	6972
1000 rpm/8 bar	-26	8	24					1420	7555
1000 rpm/6 bar	-28	6	17					1465	7374

Table 3
CKMs used in this study.

N	Author	Year	Fuel	NS/NR	TAG
1	Nakamura et al.	2017	NH3	33/232	NAK
	[38]				
2	Otomo et al. [39]	2018	NH3/H2	32/213	OTO
3	Okafor et al. [40]	2018	NH3/CH4	59/356	OKA
4	Stagni et al. [27]	2020	NH3/H2	31/203	STA
5	Bertolino et al.	2021	NH3	31/230	BER
	[41]				
6	Zhang et al. [28]	2021	NH3/H2	37/263	ZHA
7	Tamaoki et al.	2023	NH3	33/228	TAM
	[42]				
8	Zhu et al. [43]	2024	NH3/H2	43/312	ZHU
9	Liu et al. [44]	2024	NH3	30/202	LIU
10	Konnov [45,46]	2009	NH3/CH4	127/1207	KON
11	Glarborg et al.	2018	NH3/C1-C2	151/1397	GLA
	[20]			(/211)	
12	Shresta et al. [21]	2018	NH3/CH4	125/1090	SHR
13	Li et al. [26]	2019	NH3/H2/CH4	128/957	LI
14	C3MechV3.4 [47]	2023	NH3/H2/CH3OH/	3760/16553	C3M
			nC7H16		

Fig. 1 presents a simplified timeline illustrating the connections between these ammonia combustion models, highlighting how some mechanisms build upon or incorporate elements from previous ones. This emphasizes that the mechanisms, except for the originally developed ones, are modifications, adjustments, combinations, or updates of previous mechanisms. This is not exhaustive and only shows the most salient connections for illustrative purposes. In this work, each mechanism is referred to by a tag name consisting of the first three letters of the mechanism's author, as shown in Table 3. For practical purposes in this study, the 14 CKMs have been grouped into two categories. The first nine mechanisms are more compact, involving between 200 and 400 reactions, and are primarily designed to focus on ammonia oxidation. The remaining five mechanisms are more detailed, generally exceeding 1000 reactions, and incorporate sub-mechanisms addressing the oxidation of hydrocarbon species in addition to ammonia.

Adopting the nested mechanism approach of Shrestha et al. [21], a comparative overview of the sub-mechanism composition for the CKMs is presented in Table S1 of the Supplementary Information. While not exhaustive, this comparison allows for a direct assessment of each mechanism's chemical species and reaction pathways. It is important to note that this analysis considers only the chemical equations whilst kinetic parameters, thermodynamic data, and transport properties, which significantly influence a reaction's impact, are not included. With a few exceptions, the CKMs largely incorporate the same sub-mechanisms. The

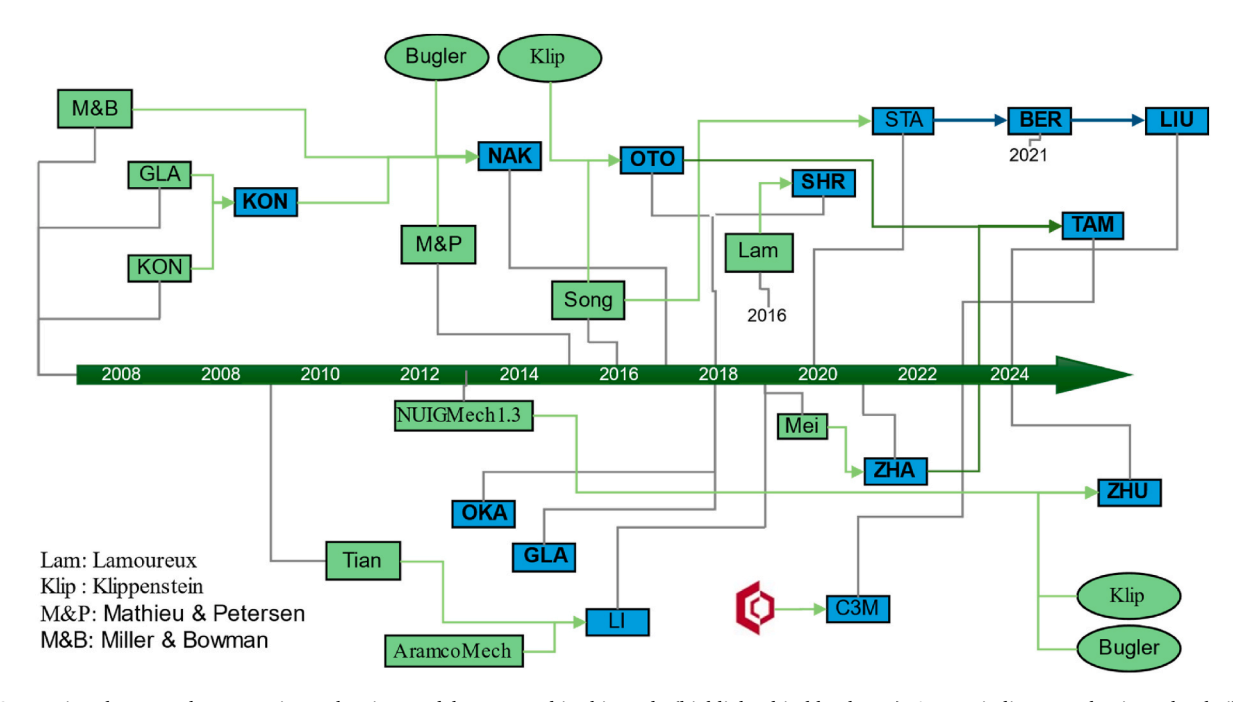


Fig. 1. Connections between the ammonia combustion models compared in this study (highlighted in blue boxes). Arrows indicate mechanisms that built upon or incorporated elements from previous ones. (For interpretation of the references to colour in this figure legend, the reader is referred to the Web version of this article.)

Zeldovich mechanism is part of all CKMs. This is the mechanism that initiates the decomposition of  $N_2$  in air to NO. Zhu et al. stands apart by including the HNNO sub-mechanism from Meng et al. [48]. This sub-mechanism, derived from ab initio (based on fundamental principles) kinetics, is expected to enhance NOx prediction by accounting for both the stabilization of  $N_2O+H$  and the oxidation of HNNO. Conversely, the mechanism by OKA omits several sub-mechanisms (NH<sub>2</sub>OH, H<sub>2</sub>NO, HNOH, HONO/HNO<sub>2</sub>, and HNNO), potentially impacting its predictive capability.

#### 4. Engine modelling approach

The ANSYS® Chemkin-Pro 2023 R1 0-dimensional model was used to simulate the internal combustion engine. The engine model used a two-zone thermodynamic model to simulate the combustion process. The two-zone thermodynamic model divides the combustion chamber into burned and unburned zones separated by the flame front. This model simulates the dynamic process of combustion, considering that the flame propagation converts the fresh mixture in the unburned zone into combustion products that fill the burned zone. In this model the reaction takes place in the flame front. In this two-zone thermodynamic model the mass exchange between zones (combustion law) is governed by the Wiebe function [49]. It quantifies the mass fraction of fuel burned (MFB) as a function of combustion efficiency ( $f_{\rm comb}$ ), start of combustion and combustion duration (SoC and Dur, respectively), as described in Equation (1).

$$MFB = \frac{m_b}{m_{total}} = f_{comb} \left( 1 - e^{-b} \left[ \frac{CAD - SoC}{Dur} \right]^{n+1} \right)$$
 Equation 1

The parameters b and n were determined by fitting the simulated pressure-crank angle degree (P-CAD) curve to the experimental pressure-CAD data. The experimental pressure data was averaged over 300 cycles and exhibited an IMEP Coefficient of Variation (CoV) lower than 3 % for each test point in Table 2. The fitting process was performed using a nonlinear least-squares optimization algorithm. This approach is a common practice in engine modelling studies, with examples applied to a variety of alternative fuels [50-52], and ensures that the Wiebe function, despite its 0D formulation, implicitly captures the net effect of complex in-cylinder phenomena on the overall combustion progression as reflected in the experimental pressure trace, leading to a suitable representation of the heat release rate. The combustion efficiency was also adjusted to align the simulated unburned ammonia with the experimentally observed ammonia slip values (provided in Table 2). The complete set of resulting Wiebe parameters and other pertinent data for each operating condition is available in Table S2 of the Supplementary Information.

The heat transfer coefficient profile (h) within the combustion chamber was determined using the correlation of Woschni [53] (Equation (2)). This correlation considers the dynamic increase in gas velocity during combustion which provides a more reliable estimate of the convective heat transfer coefficient compared to correlations that assume constant gas velocity. Equation (2) relates h to the cylinder bore (B, from Table 1), instantaneous cylinder pressure (p) and temperature (T), and mean piston speed (cm).

$$\label{eq:hamiltonian} \textit{h} = 130 k_w B^{-0.2} p^{0.8} T^{-0.53} \bigg[ C_1 c_m + C_2 \frac{V_D T_0}{p_0 V_0} (p-p_0) \bigg]^{0.8} \hspace{1cm} \text{Equation 2}$$

In Equation (2), the other parameters include the volume displaced per cylinder ( $V_D$ , the swept volume), and cylinder volume at intake valve closing ( $V_0$ , the total volume in the cylinder when the intake valve shuts), pressure ( $p_0$ ), and temperature ( $T_0$ ) at IVC.  $C_1$  accounts for the ratio of instantaneous flame propagation speed to mean piston speed, and  $C_2$  distinguishes between direct injection (DI) and indirect injection (IDI) engine types. For this simulation,  $C_1$  and  $C_2$  were set to 2.28 and

 $0.00324\ [54]$ , respectively, and the adjustment constant  $k_W$  was estimated to be 0.9.

#### 5. Results and discussion

#### 5.1. NOx formation

Fig. 2 compares predicted NO<sub>X</sub> emissions from the CKMs with experimental data for the twelve ammonia-fueled SI engine conditions in Table 2. Generally, all the mechanisms studied reproduced NO<sub>X</sub> emissions within the same order of magnitude as the experimental values. The maximum error observed was 20 % (for Zhang at 1000 rpm/ 10 bar), although the average error was less than 10 %, a deviation larger than the  $\sim$ 1–2 % experimental uncertainty. At high speeds and low loads (lower temperatures), NO<sub>X</sub> formation or destruction could predominantly occur in the final stages of the engine cycle, potentially influenced by higher ammonia slip concentrations (see Table 2). The models may not fully capture this late-cycle NO<sub>X</sub> formation, leading to underestimation. Conversely, at lower speeds, longer reaction times could allow for NO<sub>X</sub> overproduction by the mechanisms. Throughout this comparison of NOx prediction, the average error in IMEP prediction remained approximately 12 %, indicating a reasonable overall thermodynamic prediction capability of the models.

An evaluation of  $NO_X$  prediction deviations highlighted the relative accuracy of KON (lowest MAE  $\sim$  83 ppm) and STG (strong agreement at lower speeds). Specifically, STG's accuracy appeared better at lower engine speeds (e.g., 1000 rpm), potentially due to longer in-cylinder residence times allowing for more complete reaction modelling. Conversely, ZHA and GLA tended to overestimate NOx, while CTM and ZHU showed substantial underpredictions (variabilities of 130 ppm and 127 ppm, respectively), particularly at higher engine speeds where the representation of high-temperature reaction pathways might be more critical

When comparing the performance of simpler and more complex kinetic mechanisms as groups, the latter (KON, GLA, SHR, LI, CTM) exhibit a slight lower bias and reduced variability, indicating more stable and accurate predictions overall, suggesting that the additional kinetic details help mitigate systematic underprediction. Furthermore, the standard deviation of errors was notably lower for the complex mechanisms, reflecting improved consistency. However, certain simpler mechanisms, such as OKA and BER, achieved competitive accuracy in specific conditions, particularly at intermediate and low loads. This suggests that while increased kinetic complexity generally improves NOx prediction, some well-optimized compact mechanisms can still provide reasonable accuracy with a more manageable computational cost. A persistent challenge in combustion modelling is navigating the trade-off between kinetic accuracy and computational speed, a limitation especially pronounced in resource-intensive CFD simulations [55]. Indeed, direct comparisons for specific engine applications, such as methanol combustion, have shown that carefully selected and calibrated reduced mechanisms can successfully replicate experimental data [56]. Such findings validate the community's broader effort to build comprehensive, hierarchical libraries of kinetic sub-models from which tailored, efficient mechanisms for practical use can be derived [57].

Alongside  $NO_X$ ,  $N_2O$  is a critical emission from ammonia combustion due to its high global warming potential. Although  $N_2O$  was not measured in the source experimental campaign [36], preventing a direct validation, its formation was estimated using all 14 evaluated CKMs. The simulations revealed a stark divergence in predictive capability: thirteen of the mechanisms predicted negligible  $N_2O$  concentrations, typically below 1 ppm. The sole exception was the Konnov mechanism, which predicted engine-out  $N_2O$  levels in the range of 14–24 ppm across the tested conditions. While these remain unvalidated predictions, this finding is significant when contextualized with recent experimental work. Studies on comparable pure ammonia SI engines have reported measured  $N_2O$  emissions in the range of 20–80 ppm [58] and below 50

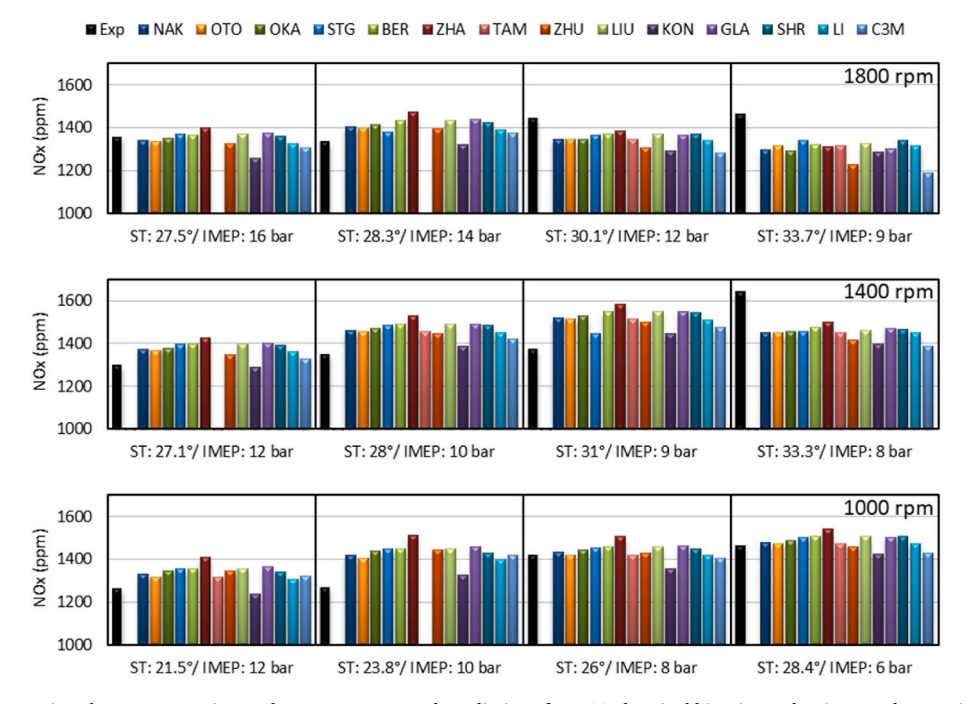


Fig. 2. NOx emissions comparison between experimental measurements and predictions from 10 chemical kinetic mechanisms under varying spark timings (ST) and indicated mean effective pressures (IMEP) for a spark-ignition (SI) engine at different engine speeds (1800, 1400, and 1000 rpm).

ppm [59]. This external evidence suggests that the near-zero predictions from most mechanisms may be inaccurate, and that the Konnov mechanism, initially an outlier, provides the most plausible order-of-magnitude prediction for  $N_2O$  formation under these conditions.

While the preceding analysis provides a preliminary assessment of the CKMs' accuracy based solely on  $NO_X$  predictions, a more comprehensive evaluation should consider their ability to capture the interplay between engine performance and emissions. Therefore, a Multi-Response Signal-to-Noise (MRSN) analysis, grounded in the Taguchi method [60], was conducted to assess the CKMs' capacity to holistically predict these interconnected aspects. This approach facilitates a robust comparison by simultaneously evaluating the accuracy of  $NO_X$ ,  $NH_3$ , and IMEP predictions, ultimately identifying the mechanism that best captures the overall combustion behaviour. The percentage errors for  $NO_X$ ,  $NH_3$ , and IMEP for each kinetic mechanism was calculated as per Equation (3).

$$\% Error = 100 \left( \frac{\textit{Value}_{\textit{Simuladed}} - \textit{Value}_{\textit{Experimental}}}{\textit{Value}_{\textit{Experimental}}} \right) \hspace{1cm} \text{Equation 3}$$

The percentage error for the  $NO_x$ ,  $NH_3$ , and IMEP predictions was calculated for each kinetic mechanism across all operating conditions. A detailed summary of this error analysis is presented in Table S3 of the Supplementary Information. From these results, it can be observed that the relative percentage error falls within  $\pm 20$  %. This indicates that the predictive capacity of all evaluated mechanisms is within the same order of magnitude as the corresponding experimental measurements. The MRSN ratio approach was used to identify the most suitable mechanism among the nine grouped in the first cluster (with similar numbers of species and reactions) for predicting engine performance and emissions. It is important to note that the Tamaoki (TAM) mechanism could not achieve convergence in the simulations for some of the tested operating conditions (see Table 2), therefore was excluded from the subsequent MRSN analysis.

The MRSN approach involves calculating a signal-to-noise ratio that considers the deviation of each response variable from the desired outcome. To quantify the deviation from the desired outcome, a loss function was defined for each response variable. The loss function is a

measure of the discrepancy between the predicted value and the experimental value. A higher value of the loss function signifies a greater deviation from the desired outcome. Given that the objective is to minimize the prediction error for all three response variables, the loss function was defined as 'lower-is-better' [60]. Mathematically, the loss function for each response variable was calculated according to Equation (4).

$$L_{ijk} = \left(y_{ijk} - y_{target}\right)^2$$
 Equation 4

Where,  $L_{ijk}$  and  $y_{ijk}$  represents the loss function and deviation in predicted output compared to the experimental outcome, respectively for the ith mechanism, jth response variable (NO<sub>X</sub>, NH<sub>3</sub>, or IMEP) and kth operating condition Also,  $y_{target}$  is the target value deviation in output for response variable in consideration. In this case  $y_{target}$  is zero as the ideal mechanism would produce no deviation in output when compared to the experimental outcome. The MRSN is then calculated as in Equation 5.

$$MRSN = -10 \times log_{10} \left( \sum w_j S_{ij} \right)$$
 Equation 5

Where,  $\sum w_{ij}S_{ij}$  represents the weighted normalized loss function. It is computed by multiplying an assigned weighting factor  $(w_j)$  (to each of the response variables) with the normalized loss function  $(S_{ij})$ , as shown in Equation (6).

$$S_{ij} = \sum_{k=1}^{n} L_{ijk} / L_{avg}$$
 Equation 6

Where  $L_{ijk}$  is total loss function (ith mechanism, jth response variable and kth operating condition) and  $L_{avg}$  is the average loss function for jth response variable. Weighting factors ( $w_j$ ) enable the prioritization of different response variables. In this study,  $w_j$  values were assigned as follows: 0.45 for NO<sub>X</sub>, 0.10 for NH<sub>3</sub>, and 0.45 for IMEP. This distribution reflects the emphasis placed on accurately predicting NO<sub>X</sub> and IMEP, aligning with the primary focus of this research. NH<sub>3</sub>, while assigned a lower weight of 0.10, served as a calibration criterion, thus explaining the observed low error values despite its reduced weighting. The results in Table 4 show the total loss function, normalized loss function, and the

**Table 4**MRSN analysis to identify optimum reaction mechanism in the first group.

CKM	Total los $L_{ij} = \sum_{ij} $	s function $\sum_{k=1}^{n} L_{ijk}$		Normal $S_{ij} = \frac{1}{L}$	MRSN		
	NO <sub>x</sub>	NO <sub>x</sub> NH <sub>3</sub> IMEP		$NO_x$	NH <sub>3</sub>	IMEP	Total
NAK	0.069	0.0002	0.197	0.84	1.00	1.06	0.20
ОТО	0.061	0.0001	0.179	0.75	0.88	0.96	0.66
OKA	0.077	0.0002	0.180	0.94	1.04	0.97	0.15
STA	0.062	0.0002	0.194	0.77	1.14	1.04	0.33
BER	0.081	0.0001	0.186	0.99	0.88	1.00	0.06
ZHA	0.129	0.0002	0.179	1.58	1.00	0.96	-0.95
ZHU	0.091	0.0002	0.180	1.11	1.13	0.97	-0.21
LIU	0.083	0.0002	0.191	1.02	0.92	1.03	-0.05
$L_{avg}$	0.082	0.0002	0.186				

final MRSN value for each mechanism. Reaction mechanisms with higher MRSN values indicate better predictive capabilities. Under the operating conditions investigated, the Otomo mechanism (OTO in Table 4) exhibited the best overall predictive capability. This suggests that Otomo effectively balances accuracy across NOX, NH3 and IMEP, making it a robust and reliable CKM for simulating ammonia combustion in SI engines. The Stagni and Nakamura mechanisms also demonstrated strong predictive capabilities, ranking second and third. Interestingly, the Zhang, Zhu, and Liu mechanisms, despite being more recent developments (see Fig. 1), yielded the lowest MRSN values. This may indicate that these mechanisms are better suited for different operating conditions or fuel compositions than those considered in this study. It is therefore acknowledged that this ranking is specific to the stated research objectives, and that a different set of weighting factors—prioritizing other outputs such as NH3 slip or any other performance metric-could potentially lead to a different hierarchy of the mechanisms.

While a previous analysis suggested that more complex mechanisms generally exhibit greater accuracy in NO<sub>X</sub> prediction, a closer examination of the prediction errors reveals a more nuanced picture. Specifically, the increased complexity of mechanisms did not show a significant improvement in prediction accuracy compared to compact mechanisms. This observation aligns with a recurring theme in combustion modelling. While detailed mechanisms are foundational, their computational cost often makes them impractical for complex engine simulations, creating a need for robust, compact surrogate models that capture the essential physics for real-world applications [61]. Furthermore, direct comparisons for fuels like methane/hydrogen blends have shown that well-designed reduced mechanisms can provide excellent agreement with experimental data, demonstrating that increased complexity does not always guarantee superior predictive accuracy [62]. In addition, the procedure to compare mechanisms (i.e., MRSN) was applied once more, taking into consideration the three most effective mechanisms from the first group (Otomo, Stagni, and Nakamura)

**Table 5**MRSN analysis to identify optimum reaction mechanism.

CKM		ss function $\sum_{k=1}^{n} y_{ijk}^{2}$		$S_{ii} = \frac{1}{2}$	Normalized loss function $S_{ij} = rac{L_{ij}}{L_{avg}}$				
	NO <sub>x</sub>	NH <sub>3</sub>	IMEP	$NO_x$	$NH_3$	IMEP	Total		
NAK	0.069	0.0002	0.197	0.96	0.53	1.06	0.16		
ОТО	0.061	0.0001	0.179	0.86	0.47	0.97	0.62		
STA	0.062	0.0002	0.194	0.88	0.61	1.04	0.34		
KON	0.062	0.0002	0.178	0.87	0.51	0.96	0.57		
GLA	0.089	0.0002	0.186	1.25	0.48	1.00	-0.25		
SHR	0.071	0.0008	0.185	1.00	2.41	1.00	-0.57		
LI	0.058	0.0007	0.183	0.82	2.34	0.99	-0.19		
C3M	0.097	0.0002	0.182	1.37	0.65	0.98	-0.50		
$L_{avg}$	0.071	0.0003	0.185						

and all the mechanisms from the more complex mechanism group (Table 5). The results demonstrate that, under the study conditions, the Otomo mechanism yielded the most effective results, followed by Konnov and Stagni. This finding reinforces the previously mentioned assertion that the increased complexity of these mechanisms does not necessarily result in superior outcomes.

#### 5.2. Rate of production analysis of NO

Rate of production (ROP) analysis was employed to investigate the temporal evolution of net NO production throughout the combustion cycle. Fig. 3 illustrates the calculated net NO ROP, as derived from the chemical kinetic mechanism of Otomo et al. [39].

Notably, Fig. 3 demonstrates the occurrence of inverse NO generation trajectories between approximately 20-30 CAD (depending on the spark timing), coinciding with the peak cylinder temperature. After the peak cylinder temperature, reactions consuming NO are accelerated, and/or the reactions producing NO shift towards consumption. This culminates in a reduction of NO concentration during the later stages of combustion and the subsequent post-combustion phase. Comparing engine operating conditions, a consistent trend of decreasing NO ROP with reducing engine load was observed across all engine speeds. This trend is directly attributable to the corresponding decrease in peak combustion temperatures, which mitigates thermal NO<sub>X</sub> formation. It is noted that the more advanced spark timing required at lower loads (see Table 2) can locally increase peak temperatures, which would promote NOx formation. However, the dominant effect observed in the net production rate is the overall reduction in temperature due to the lower engine load. Reducing residence time within the high-temperature combustion chamber because of elevated engine speeds (e.g. 1800 rpm in Fig. 3) reduced the NO formation rate.

Beyond the overall trends, a comparative analysis of different CKMs was undertaken to assess their predictive capabilities for NO ROP. The seven most influential reactions contributing to both NO formation (positive ROP) and consumption (negative ROP) were identified. This analysis was extended to the three highest-ranked mechanisms (Otomo, Nakamura, Stagni) according to a Taguchi analysis (in section 5.1), and for comparative purposes, also applied to the three lowest-ranked mechanisms) (Zhang, Zhu, and Liu). A list of these key reactions and their corresponding identifiers within each mechanism is provided in Table S4 of the Supplementary Information. In this, a nomenclature links each reaction to its respective mechanism, even though these reactions may also be present in other mechanisms. For instance, reaction 63 in the Otomo mechanism (OTO-R63, NH + NO↔N2O + H) corresponds to reactions NAK-R43, STA-R85, ZHA-R51, ZHU-R93, and LIU-R514 in the Nakamura, Stagni, Zhang, Zhu, and Liu mechanisms, respectively. Fig. 4 presents the NO ROP for two selected engine operating conditions (1800 rpm/12 bar, representing a higher engine speed with moderate load, and 1000 rpm/10 bar, representing a lower speed with similar relative load within tested range). The remaining tested conditions exhibiting similar overall behaviour.

The Zeldovich sub-mechanism, responsible for thermal- $NO_X$  formation, plays a critical role in all cases and mechanisms examined, highlighting its significance in overall  $NO_X$  production.

As shown in Fig. 4, the two most influential reactions are N + NO $\rightleftharpoons$ N<sub>2</sub>+O (identified as OTO-R70, STA-R91, ZHA-R40, ZHU-R100, and LIU-R503) and N + OH $\rightleftharpoons$ NO + H (present as OTO-R68, NAK-R98, STA-R89, ZHA-R39, ZHU-R98, and LIU-R502). Of these, N + NO $\rightleftharpoons$ N<sub>2</sub>+O exhibits the highest ROP across all cases. This reaction, significantly contributes to NO formation, followed by N + OH $\rightleftharpoons$ NO + H, indicating a substantial presence of OH radicals. The highly endothermic reaction N + O<sub>2</sub> $\rightleftharpoons$ NO + O reaches its maximum ROP at the point of maximum temperature rise, as expected, and subsequently decreases. As the combustion chamber temperature drops, this reaction slows down and eventually reverses, favouring the dissociation of NO into N and O<sub>2</sub>. Importantly, the observed variability in NO<sub>X</sub> predictions across different

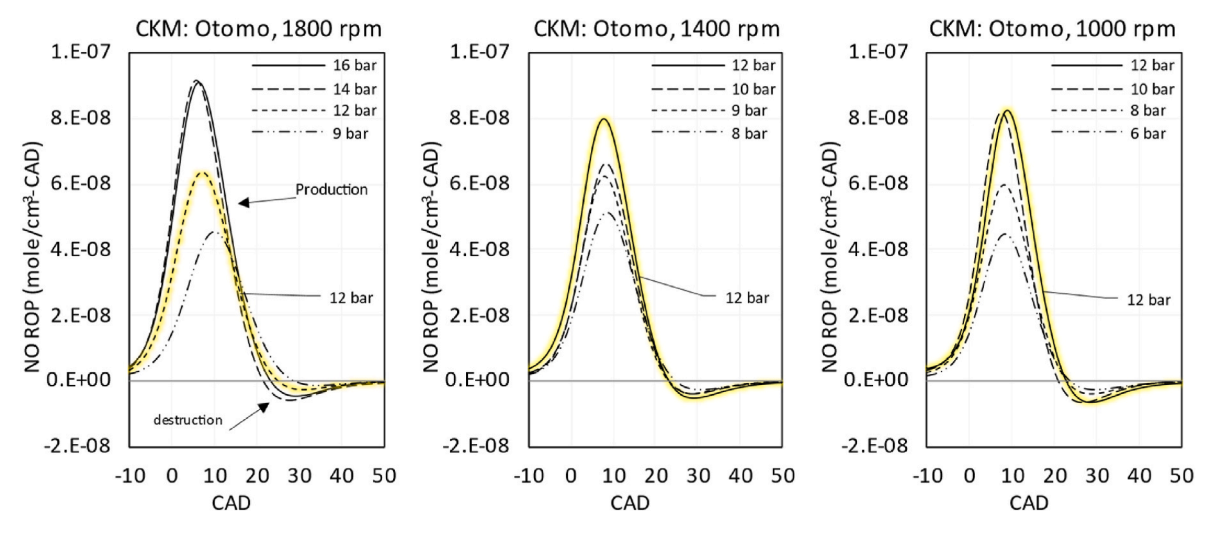


Fig. 3. Net NO Rate of Production (ROP) profiles under varying engine operating conditions, as predicted by the Otomo CKM (IMEP 12 bar line highlighted).

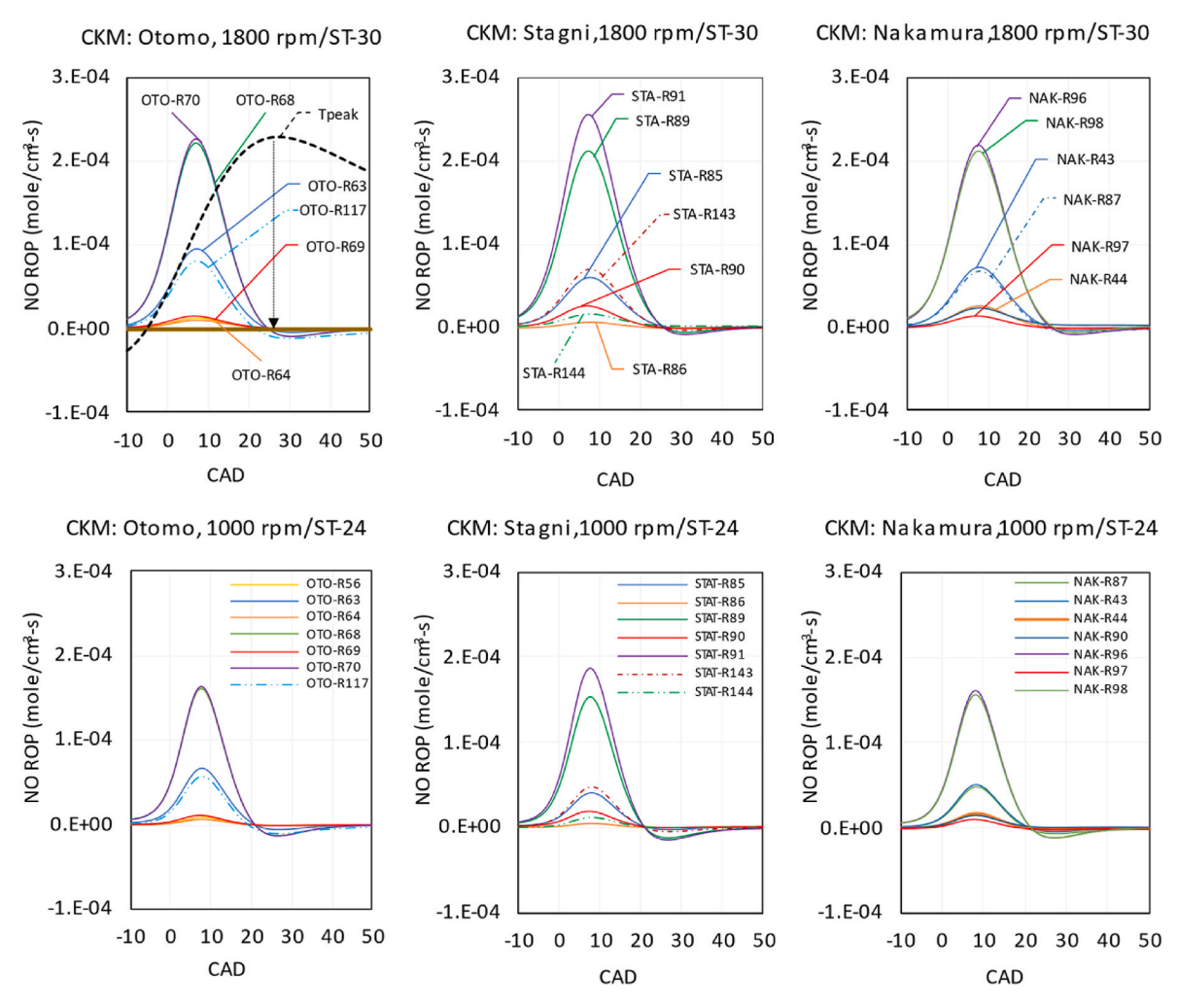


Fig. 4. Rate of production of NO 1800 rpm/12 bar (top) and 1000 rpm/10 bar (bottom) by the 3 top CKMs: Otomo (left), Nakamura (middle) and Stagni (right).

CKMs can be partially attributed to inconsistencies in the kinetic rate constants of each mechanism, as highlighted by Meulemans et al. [63]. They demonstrate that such discrepancies are a direct consequence of uncertainty in Arrhenius rate parameters (primarily the pre-exponential factor (A) and the activation energy (Ea)). Fig. 5 compares the kinetic rates for the key reactions involved in thermal-NO $_{\rm X}$  formation across the

evaluated mechanisms, showing discrepancies, particularly in the reactions  $N+NO{\rightleftharpoons}N_2{+}O$  and  $N+OH{\rightleftharpoons}NO+H.$ 

Furthermore, according to the ROP, the HNO sub-mechanism is relevant to NO formation as some of the reactions in it are among the seven most important. These primarily involve HNO decomposition, as in  $\text{HNO} \rightleftharpoons \text{H} + \text{NO}$  (STA-R143), and hydrogen abstraction by H and OH,

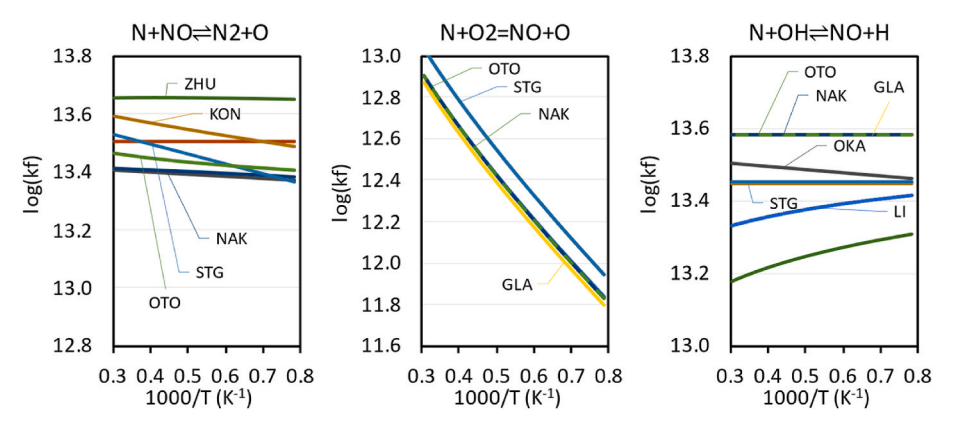


Fig. 5. Comparison of the reaction rate constants for the key reactions involved in thermal-NOx formation across the chemical kinetic mechanisms (CKMs) evaluated in this study.

yielding NO and  $H_2$ ,  $H_2O$ , or  $HO_2$ , respectively, like  $HNO + H \rightleftharpoons NO + H_2$ (STA-R144). This is evidence that this sub-mechanism demands careful consideration when refining mechanisms involving NH3 oxidation. Fig. 4 also reveals the importance of the reactions NH + NO $\rightleftharpoons$ N<sub>2</sub>O + H (OTO-R63) and NH + NO⇒N<sub>2</sub>+OH (OTO-R64) in nearly all chemical kinetic mechanisms, although the latter does not appear among the most important reactions in the ZHU and LIU mechanisms. This may explain the average deviation in their performance compared to the other CKMs. The presence of the reaction OTO-R63, the third largest contributor to NO production in most mechanisms, in all cases suggests that the coupled effect of both reactions within the N2O sub-mechanism (as detailed in Table S1 of the Supplementary Information) is fundamental, influencing both NO formation and consumption. N2O can decompose to produce O atoms, which then participate in chain-branching reactions that increase the radical pool ( $H_2+O \rightleftharpoons H + OH$ ), ultimately impacting NO formation.

The ROP analysis confirmed that pathways involving other nitrogenous species such as  $NH_2OH$  and  $H_2NO$ , while present in several mechanisms as detailed in Table S1, had a minor contribution to the net NO production rate. Thus, they are not analysed in further detail.

## 5.3. Thermal NOx and fuel NOx

To quantify the individual contributions of thermal-NO<sub>x</sub> and fuel NO<sub>X</sub>, a full kinetic simulation was performed using the nitrogen isotope labelling method was applied, a technique whose implementation in multi-dimensional CFD has been recently detailed [34] and has been used to investigate NOx sources in various engine concepts, including ammonia-diesel dual-fuel systems [36] and other ammonia spark-ignition configurations [35]. Each CKM was modified by introducing a nitrogen isotope (i.e., N\*) and replicating every reaction involving nitrogen to include all possible combinations of N and N\*. This included replicating the contribution of N2 as a third body for each reaction where it is considered. Similarly, the thermodynamic and transport properties are replicated. For instance, a key thermal-NOx reaction such as N + OH ≠ NO + H was complemented by its isotopic equivalent,  $N^*+OH\rightleftharpoons N^*O+H$ , to track the fuel-based pathway. This systematic duplication was applied to all nitrogen-bearing reactions. In the new reactions, the Arrhenius parameters of the original reactions are maintained. This ensured that both atmospheric nitrogen (N) and the fictitious isotope originating from NH<sub>3</sub> (N\*) had equal opportunities to react within the pool of reactions. By tracking the formation of conventional  $NO_X$  (NO,  $NO_2$ ) and the isotopically labelled  $N^*O_X$  (N\*O, N\*O2), it was possible to distinguish between thermal NO<sub>X</sub> (originating from atmospheric N<sub>2</sub>) and fuel NO<sub>X</sub> (derived from NH<sub>3</sub>). This approach allowed for a detailed analysis of the individual contributions of each NO<sub>X</sub> source while maintaining the integrity of the reaction kinetics. Thus, for each CKM used-referred to as CKM\_reg (regular or original)-a

corresponding modified chemical kinetic mechanism (CKM $\_$ mod) was created.

A critical prerequisite for the isotopic analysis was to confirm that the modifications to the kinetic mechanism did not impact the model's bulk thermodynamic behaviour. To this end, we compared the incylinder pressure and apparent heat release rate (AHRR) profiles from the modified CKM against both the original mechanism and experimental measurements. The resulting plots, provided in Fig. S1 of the Supplementary Information, reveal a near-perfect overlay of the pressure and AHRR traces from both the regular and modified mechanisms. This visual evidence, supported by R-squared values consistently above 0.94 for pressure, affirms that the isotopic labelling approach preserves the thermodynamic integrity of the simulation

Fig. 6 details the modelled net formation of fuel-NO<sub>X</sub> and thermal-NO<sub>X</sub> as they evolve over the engine's crank angle, according to the modified chemical kinetic mechanism. The red line in the same plots illustrates the combined contribution of these two NO<sub>X</sub> pathways according to the modified mechanism. For direct comparison, the total NOx predicted by the regular CKM is also presented. Alongside these modelled results, yellow star markers indicate the experimentally measured NOx values under the investigated conditions. Fuel-NO<sub>X</sub> formation is initiated earlier in the combustion process; however, thermal-NO<sub>X</sub> formation consistently dominates, exceeding fuel-NO<sub>X</sub> contributions, consistent with the previous ROP analysis highlighting dominant Zeldovich reactions. Fuel-NOx starts earlier, but thermal-NOx dominates, as anticipated from the previous ROP analysis highlighting the critical role of the Zeldovich sub-mechanism in total NOx formation across all cases and mechanisms. This is clearly illustrated in the case of Nakamura at 1800 rpm/12 bar (although observed in all cases). Such delayed formation of thermal-NO<sub>X</sub> is attributed to its dependence on achieving high temperatures, whereas fuel-NO<sub>X</sub> is generated during the earlier stages of ammonia degradation. The modified mechanisms consistently predict total- $NO_X$  (thermal- $NO_X$  + fuel- $NO_X$ ) levels that are 10 %-15 % higher than those predicted by the regular CKM. This observation aligns with the findings of Sun et al. [64] for ammonia-diesel mixtures, and Yang et al. [34], who attributed similar increases to the decoupling of NO<sub>X</sub> sources in the modified mechanism. Regarding the comparison with experimental NO<sub>X</sub> values, the predicted NO<sub>X</sub> from the three compared mechanisms underestimates the experimental data at 1800 rpm but overestimates it at 1000 rpm.

The approach of decoupling eliminates the interdependence and competition for radicals inherent in the coupled system. While the coupled mechanism allows for shared radical pools and thus a natural regulatory effect on  $NO_X$  formation, the decoupled mechanism segregates these pools, removing this regulatory influence consequently leading to higher total  $NO_X$  predictions. Although this work employed a comprehensive duplication of reactions to ensure both nitrogen species (N and N\*) had access to all possible reactions, mimicking the behaviour

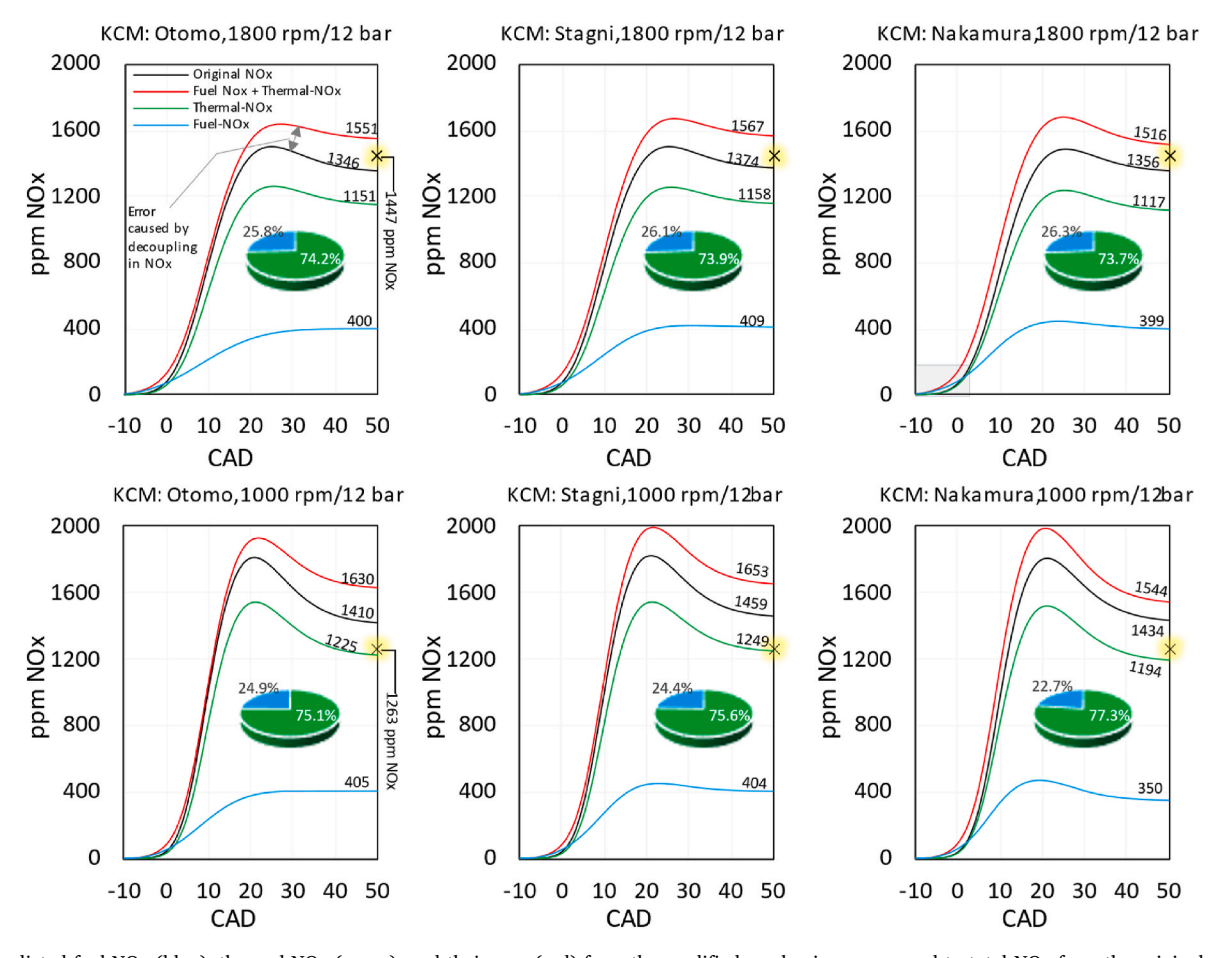


Fig. 6. Predicted fuel-NOx (blue), thermal-NOx (green), and their sum (red) from the modified mechanism, compared to total  $NO_X$  from the original mechanism (black) and experimental values (yellow stars). Pie charts indicate the thermal/fuel- $NO_X$  fractions from the modified mechanism. (For interpretation of the references to colour in this figure legend, the reader is referred to the Web version of this article.)

of N atoms in the regular CKM, an error was still observed. This aligns with the explanation provided by Yang et al. [34], where the decoupling effect inhibits the inherent suppression of  $NO_X$  formation present in the regular, coupled mechanism. Despite this discrepancy in total- $NO_X$  (the error introduced by  $NO_X$  decoupling), it is considered acceptable for determining the relative contributions of thermal- and fuel- $NO_X$ .

Table 6 provides a broader picture in terms of the engine conditions tested for the three selected mechanisms. It shows the percentages of fuel-NO<sub>X</sub> and thermal-NO<sub>X</sub> (calculated based on the concentration of NO<sub>X</sub> at the end of combustion) and the decoupling error in NO<sub>X</sub>. In general terms, the mechanisms used produce similar and consistent results. The findings suggest that under the investigated conditions, thermal-NO<sub>X</sub> accounts for around 75  $\pm$  2 % of the total NO<sub>X</sub> emissions

(averaged by CKM), thus indicating that the remaining 25 % is attributable to fuel-NO $_{\rm X}$ . Averaged across the tested CKMs, the Nakamura mechanism showed a slightly lower decoupling error for total NO $_{\rm X}$  compared to the others, suggesting a slightly higher accuracy for this type of analysis, particularly at very low engine speeds.

Table 6 reveals consistent trends across all operating conditions (speed and load) and CKMs. The data indicates no statistically significant variations in fuel-NO $_{\rm X}$  and thermal-NO $_{\rm X}$  percentages between these scenarios. Thus, even with the use of pure ammonia as fuel, thermal-NO $_{\rm X}$  continues to represent the largest source of NO $_{\rm X}$ , which suggests that strategies such as staged combustion [65], exhaust gas recirculation, or moderate or intense low-oxygen dilution combustion could potentially help mitigate these emissions, as they aim to lower the peak combustion

Table 6
Fuel NOx contributions to total NOx emissions, predicted using the Otomo, Stagni, and Nakamura kinetic mechanisms for all experimental conditions.

CKM		1800 rpm				1400 rpm			1000 rpm				AVG	SD	
	MEP T (°C)	16 bar	14 bar	12 bar	9 bar	12 bar	10 bar	9 bar	8 bar	12 bar	10 bar	8 bar	6 bar		
		C) 2137	2112	2078	2005	2092	2053	2014	1973	2028	2014	1925	1785		
ОТО	Fuel-NOx	25.2 %	24.8 %	25.9 %	25.9 %	25.5 %	24.8 %	24.5 %	25.5 %	25.6 %	25.0 %	25.1 %	25.1 %	25.2 %	0.5 %
	Thermal-Nox	74.8 %	75.2 %	74.1 %	74.1 %	74.5 %	75.2 %	75.5 %	74.5 %	74.4 %	75.0 %	74.9 %	74.9 %	74.8 %	0.5 %
	ErrorDecoup	12.6 %	12.2 %	12.8 %	12.8 %	12.7 %	12.2 %	11.8 %	12.2 %	13.5 %	13.2 %	12.8 %	12.5 %	13 %	0 %
STG	Fuel-NOx	25.2 %	25.1 %	26.1 %	27.4 %	25.4 %	24.9 %	24.7 %	25.7 %	24.7 %	24.5 %	24.8 %	25.1 %	25.3 %	0.8 %
	Thermal-Nox	74.8 %	74.9 %	73.9 %	72.6 %	74.6 %	75.1 %	75.3 %	74.3 %	75.3 %	75.5 %	75.2 %	74.9 %	74.7 %	0.8 %
	ErrorDecoup	11.8 %	11.8 %	12.3 %	12.5 %	11.9 %	11.5 %	11.3 %	11.8 %	11.8 %	11.7 %	11.7 %	11.8 %	12 %	0 %
NAK	Fuel-NOx	24.5 %	24.4 %	26.3 %	28.7 %	25.0 %	24.5 %	24.3 %	26.0 %	23.1 %	22.7 %	23.7 %	24.9 %	24.8 %	1.6 %
	Thermal-NOx	75.5 %	75.6 %	73.7 %	71.3 %	75.0 %	75.5 %	75.7 %	74.0 %	76.9 %	77.3 %	76.3 %	75.1 %	75.2 %	1.6 %
	ErrorDecoup	8.7 %	8.6 %	10.5 %	13.0 %	9.2 %	8.6 %	8.5 %	10.0 %	7.4 %	7.10 %	8.0 %	9.0 %	9.0 %	2.0 %

temperatures [66]. However, with these strategies penalty on engine efficiency is expected.

#### 6. Conclusions

This study evaluated 14 ammonia combustion mechanisms within a complex spark-ignition engine environment and calibrated them against experimental data from a modified single-cylinder research engine operating on pure ammonia at stoichiometric conditions. A key aspect of this calibration was the use of experimental NH $_3$  slip data to set the combustion efficiency, thereby anchoring the model's thermodynamics to ensure a robust evaluation of NOx prediction capabilities. Understanding CKM behaviour remains relevant, as it provides key insights for optimising engine operation towards emissions reduction, even though ammonia combustion often involves co-combusting with other fuels. Although utilizing multiple CKMs is feasible, it is resource intensive. Therefore, this work offers a valuable tool for researchers and engineers seeking to model ammonia combustion in internal combustion engines, particularly in the context of NOx formation and NH $_3$  slip, by streamlining the selection process for kinetic mechanisms increasing research efficiency.

While most mechanisms captured NOX trends within 20 % of experimental values, the Otomo followed up by the Stagni and Nakamura mechanisms consistently demonstrated the strongest predictive capabilities across varying engine speeds and loads. Further analysis revealed that NO production rates consistently decrease with reducing engine load, driven by lower peak combustion temperatures. While more advanced spark timing was required at lower loads, its effect on increasing local temperatures was secondary to the overall impact of the reduced load. Conversely, NO production rates tend to increase with decreasing engine speed, potentially related to the longer residence times at lower speeds, allowing more time for NO formation reactions to

Furthermore, the analysis revealed a critical disparity in  $N_2O$  prediction among the models. Only the Konnov mechanism predicted plausible, non-negligible concentrations (14–24 ppm), a finding supported by recent experimental literature, which highlights a key deficiency in most current ammonia combustion models.

This study analyses the contributions of thermal- $NO_X$  and fuel- $NO_X$ , indicating that thermal- $NO_X$  constitutes approximately 75 % of total  $NO_X$  emissions under the investigated conditions providing guidelines on how to reduce emissions formation at the source. This work provides valuable insights into mechanism performance and  $NO_X$  formation. This study underscores the importance of mechanism validation in complex engine environments and contributes to the ongoing development of cleaner ammonia combustion technologies.

#### CRediT authorship contribution statement

A. Cova-Bonillo: Writing – original draft, Formal analysis, Data curation. P. Gabana: Formal analysis, Data curation. N. Khedkar: Formal analysis, Data curation. G. Brinklow: Writing – original draft, Validation, Methodology, Formal analysis, Conceptualization. M. Wu: Formal analysis, Data curation, Conceptualization. J.M. Herreros: Writing – review & editing, Supervision, Project administration, Funding acquisition, Conceptualization. S. Zeraati-Rezaei: Writing – review & editing, Supervision, Project administration, Funding acquisition, Conceptualization. A. Tsolakis: Writing – review & editing, Supervision, Project administration, Funding acquisition, Conceptualization. A. Ambalakatte: Formal analysis, Data curation. A. Cairns: Writing – review & editing, Supervision, Project administration, Funding acquisition, Data curation. J. Hall: Writing – review & editing, Supervision.

### Declaration of competing interest

The authors declare that they have no known competing financial

interests or personal relationships that could have appeared to influence the work reported in this paper.

#### Acknowledgment

ESPRC is acknowledged for funding this work through the MariNH $_3$  project (EPSRC Ref: EP/W016656/1).

#### Appendix A. Supplementary data

Supplementary data to this article can be found online at https://doi.org/10.1016/j.ijhydene.2025.150734.

#### References

- Bleviss D. Transportation is critical to reducing greenhouse gas emissions in the United States. WIRES Energy Environ 2020:1–16.
- [2] Ferrer ALC, Thomé AMT. Carbon emissions in transportation: a synthesis framework. Sustainability 2023;15(11):8475.
- [3] Jafar U, Nuhu U, Khan WU, Hossain MM. A review on green ammonia as a potential CO2 free fuel. Int J Hydrogen Energy 2024;71:857–76.
- [4] Ishaq H, Crawford C. Review of ammonia production and utilization: enabling clean energy transition and net-zero climate targets. Energy Convers Manag 2024; 300:117869.
- [5] Bora N, Singh AK, Pal P, Sahoo UK, Seth D, Rathore D, Bhadra S, Sevda S, Venkatramanan V, Prasad S, Singh A, Kataki R, Sarangi PK. Green ammonia production: process technologies and challenges. Fuel 2024;369.
- [6] Moghadam MR, Bazmandegan-Shamili A, Bagheri H. Chapter one the current methods of ammonia synthesis by haber-bosch process. In: Progresses in ammonia: science; technology and membranes. Elsevier; 2024. p. 1–32.
- [7] Sforza L, Ballerini A, Ramognino F, Schirru A, Lucchini T, D'Errico G, Dupuy A, Castro RRd, Brequigny P, Mounaïm-Rousselle C. A numerical study of ammonia combustion in spark-ignition and reactive-fuel pilot-ignition engines. J Ammonia Energy 2024;2(1).
- [8] Gray J, Dimitroff E, Meckel N, Quillian R. Ammonia fuel engine compatibility and combustion. SAE Trans 1967;75:785–807.
- [9] Alnajideen M, Shi H, Northrop W, Emberson D, Kane S, Czyzewski P, Alnaeli M, Mashruk S, Rouwenhorst K, Yu C, Valera-Medina SEA. Ammonia combustion and emissions in practical applications: a review. Carb Neutrality 2024;3(13).
- [10] Hu J, Liu Y, H X, Z J, Xia S. Application of NH3 fuel in power equipment and its impact on NOx emissions. Energies 2024;17(12).
- [11] Zhu X, Du J, Yu Z, Cheng Y-B, Wang Y. NOx emission and control in ammonia combustion: State-of-the-art review and future perspectives. Energy Fuels 2024: 43–60.
- [12] Sharma V, Panesar A, Sercey Gd, Begg S. A review of ammonia combustion and emissions characteristics in spark-ignition engines and future road map. Energies 2025;18(1):41. 2025, 18(1).
- [13] Alnasif A, Mashruk S, Shi H, Alnajideen M, Wang P, Pugh D, Valera-Medina A. Evolution of ammonia reaction mechanisms and modeling parameters: a review. Appl Energy Combustion Sci 2023;15:100175.
- [14] Olm C, Zsély IG, Pálvölgyi R, Varga T, Nagy T, Curran HJ, Turányi T. Comparison of the performance of several recent hydrogen combustion mechanisms. Combust Flame 2014;161(9):2219–34.
- [15] Olm C, Zsély IG, Varga T, Curran HJ, Turányi T. Comparison of the performance of several recent syngas combustion mechanisms. Combust Flame 2015;162(5): 1793–812.
- [16] Kawka L, Juhász G, Papp M, Nagy T, Zsély IG, Turányi T. Comparison of detailed reaction mechanisms for homogeneous ammonia combustion. Z Phys Chem 2020; 234(7–9).
- [17] Mével R, Javoy S, Lafosse F, Chaumeix N, Dupré G, Paillard C-E. Hydrogen-nitrous oxide delay times: shock tube experimental study and kinetic modelling. Proc Combust Inst 2009;32(1):359–66.
- [18] Klippenstein SJ, Harding LB, Glarborg P, Miller JA. The role of NNH in NO formation and control. Combust Flame 2011;158(4):774–89.
- [19] Zhang Y, Mathieu O, Petersen EL, Bourque G, Curran HJ. Assessing the predictions of a NOx kinetic mechanism on recent hydrogen and syngas experimental data. Combust Flame 2017;182:122-41.
- [20] Glarborg P, Miller JA, Ruscic B, Klippenstein SJ. Modeling nitrogen chemistry in combustion. Prog Energy Combust Sci 2018;67:31–68.
- [21] Shrestha KP, Seidel L, Zeuch T, Mauss F. Detailed kinetic mechanism for the oxidation of ammonia including the formation and reduction of nitrogen oxides. Energy Fuels 2018;32(10).
- [22] Song Y, Marrodán L, Vin N, Herbinet O, Assaf E, Fittschen C, Stagni A, Faravelli T, Alzueta M, Battin-Leclerc F. The sensitizing effects of NO2 and NO on methane low temperature oxidation in a jet stirred reactor. Proc Combust Inst 2019;37(1): 667–75.
- [23] Kovács M, Papp M, Zsély IG, Turányi T. Determination of rate parameters of key N/ H/O elementary reactions based on H2/O2/NOx combustion experiments. Fuel 2020;264:116720.
- [24] Alnasif A, Mashruk S, Hayashi M, Jójka J, Shi H, Hayakawa A, Valera-Medina A. Performance investigation of currently available reaction mechanisms in the estimation of NO measurements: a comparative study. Energies 2023;16(9).

- [25] Rabbani S, Manias DM, Kyritsis DC, Goussis DA. Comparative review of the chemical dynamics underlying five models of ammonia fuel oxidation. Fuel 2023; 352:129063.
- [26] Li R, Konnov AA, He G, Qin F, Zhang D. Chemical mechanism development and reduction for combustion of NH3/H2/CH4 mixtures. Fuel 2019;257:116059.
- [27] Stagni A, Cavallotti C, Arunthanayothin S, Song Y, Herbinet O, Battin-Leclerc F, Faravelli T. An experimental, theoretical and kinetic-modeling study of the gasphase oxidation of ammonia. React Chem Eng 2020;5:696–711.
- [28] Zhang X, Moosakutty SP, Rajan RP, Younes M, Sarathy SM. Combustion chemistry of ammonia/hydrogen mixtures: jet-Stirred reactor measurements and comprehensive kinetic modeling. Combust Flame 2021;234.
- [29] Yuan J, Yang J, Deng J, Li L, Cai L. Comparison of chemical mechanisms for the oxidation ofhydrogen/ammonia mixtures based on different evaluationmethods. Int J Chem Kinet 2024;1(9).
- [30] Girhe S, Snackers A, Lehmann T, Langer R, Loffredo F, Glaznev R, Beeckmann J, Pitsch H. Ammonia and ammonia/hydrogen combustion: comprehensive quantitative assessment of kinetic models and examination of critical parameters. Combust Flame 2024;267:113560.
- [31] Xiao H, Valera-Medina A. Chemical kinetic mechanism study on premixed combustion of Ammonia/Hydrogen fuels for gas turbine use. J Eng Gas Turbines Power 2017;139(8).
- [32] Zhang W, Chen S, Chen Z, Li Z, Zhou M, Ma Z. A review of chemical kinetic mechanisms and after-treatment of amino fuel combustion. Sci Total Environ 2025; 959:178220.
- [33] Miller R, Davis G, Lavoie G, Newman C, Gardner T. A super-extended zeldovich mechanism for nox modeling and engine calibration. SAE Technical Paper; 1998, 980781
- [34] Yang R, Liu Z, Liu J. The methodology of decoupling fuel and thermal nitrogen oxides in multi-dimensional computational fluid dynamics combustion simulation of ammonia-hydrogen spark ignition engines. Int J Hydrogen Energy 2024;55: 300–18
- [35] Yang R, Yan Y, Liu Z, Liu J. Formation and evolution of thermal and fuel Nitrogen oxides in the turbulent combustion field of Ammonia Internal combustion engines. SAE Technical Paper; 2023. no. 2023-01-0192.
- [36] Wu B, Wang Y, Wang D, Feng Y, Jin S. Generation mechanism and emission characteristics of N2O and NOx in ammonia-diesel dual-fuel engine. Energy 2023; 284:129291.
- [37] Ambalakatte A, Hegab A, Geng S, Cairns A, Harrington A, Hall J, Bassett M. Evaluation of ammonia Co-fuelling in modern four stroke engines. Johnson Matthey Technol Rev 2024;68(3):396–411.
- [38] Nakamura H, Hasegawa S, Tezuka T. Kinetic modeling of ammonia/air weak flames in a micro flow reactor with a controlled temperature profile. Combust Flame 2017;185:16–27.
- [39] Otomo J, Koshi M, Mitsumori T, Iwasaki H, Yamada K. Chemical kinetic modeling of ammonia oxidation with improved reaction mechanism for ammonia/air and ammonia/hydrogen/air combustion. Int J Hydrogen Energy 2018;43(5):3004–14.
- [40] Okafor EC, Naito Y, Colson S, Ichikawa A, Kudo T, Hayakawa A, Kobayashi H. Measurement and modelling of the laminar burning velocity of methane-ammoniaair flames at high pressures using a reduced reaction mechanism. Combust Flame 2019;204:162-75
- [41] Bertolino A, Fürst M, Stagni A, Frassoldati A, Pelucchi M, Cavallotti C, Faravelli T, Parente A. An evolutionary, data-driven approach for mechanism optimization: theory and application to ammonia combustion. Combust Flame 2021:111366.
- [42] Tamaoki K, Murakami Y, Kanayama K, Tezuka T, Izumi M, Nakamura H. Roles of NH2 reactions in ammonia oxidation at intermediate temperatures: experiments and chemical kinetic modeling. Combust Flame 2024;259:113177.
- [43] Zhu Y, Curran HJ, Girhe S, Murakami Y, Pitsch H, Senecal K, Yang L, Zhou C-W. The combustion chemistry of ammonia and ammonia/hydrogen mixtures: a comprehensive chemical kinetic modeling study. Combust Flame 2024;260: 112330
- [44] Liu L, Tan F, Wu Z, Wang Y. Combining genetic algorithm and deep learning to optimize a chemical kinetic mechanism of ammonia under high pressure. Fuel 2024;360:130508

- [45] Konnov A, Ruyck JD. Kinetic modeling of the thermal decomposition of ammonia. Combust Sci Technol 2000;152(1):23–37.
- [46] Konnov A. Implementation of the NCN pathway of prompt-NO formation in the detailed reaction mechanism. Combust Flame 2009;156(11):2093–105.
- [47] Hamdy M, Nadiri S, Mohamed A, Dong S, Wu Y, Fernandes R, Zhou C, Liu S, Senecal K, Zhang K, Curran H. An updated comprehensive chemical kinetic mechanism for ammonia and its blends with hydrogen, methanol, and N-Heptane. SAE Technical Paper; 2023. Vols. 2023-01-0204.
- [48] Meng Q, Lei L, Lee J, Burke MP. On the role of HNNO in NO. Proc Combust Inst 2023;39(1):551–60.
- [49] Ghojel JI. Review of the development and applications of the Wiebe function: a tribute to the contribution of Ivan Wiebe to engine research. Int J Engine Res 2010; 11(4):297–312.
- [50] Diaz GJA, Montoya JPG, Martinez LAC, Olsen DB, Navarro AS. Influence of engine operating conditions on combustion parameters in a spark ignited internal combustion engine fueled with blends of methane and hydrogen. Energy Convers Manag 2019;181:414–24.
- [51] Xie M, Li Q, Fu J, Yang H, Wang X, Liu J. Chemical kinetic investigation on NOx emission of SI engine fueled with gasoline-ethanol fuel blends. Sci Total Environ 2022;831:154870.
- [52] Isobe K, Yoshimura K, Kobayashi T, Sok R, Kusaka J. Impacts of low-temperature heat release on unstretched laminar burning velocity in advanced flex-fuel gasoline-ethanol engines. Appl Therm Eng 2025;258:124826.
- [53] Woschni G. A universally applicable equation for the instantaneous heat transfer coefficient in the internal combustion engine. SAE Technical Paper; 1967, 670931.
- [54] Fagundez J, Sari R, Martins M, Salau N. Comparative analysis of different heat transfer correlations in a two-zone combustion model applied on a SI engine fueled with wet ethanol. Appl Therm Eng 2017;115:22–32.
- [55] Zettervall N, Fureby C, Nilsson EJK. Evaluation of chemical kinetic mechanisms for methane combustion: a review from a CFD perspective. Fuel 2021;2(2):210–40.
- [56] Pucilowski M, Li R, Xu S, Li C, Qin F, Tuner M, Bai X-S, Konnov AA. Comparison of kinetic mechanisms for Numerical Simulation of methanol combustion in DICI heavy-duty engine. SAE Technical Paper; 2019. Vols. 2019-01-0208.
- [57] Pelucchi M, Cai L, Pejpichestakul W, Tripathi R, Wagnon S, Zhang K, Raju M, Mehl M, Faravelli T, Pitz W, Pitsch H, Curran H, Senecal PK. Computational chemistry consortium: surrogate fuel mechanism development, pollutants submechanisms and components Library. SAE Technical Paper 2019;2019-24-0020.
- [58] Jespersen MC, Rasmussen TØH, Ivarsson A. Widening the operation limits of a SI engine running on neat ammonia. Fuel 2024;358(B).
- [59] Mounaïm-Rousselle C, Bréquigny P, Dumand C, Houillé S. Operating limits for ammonia fuel spark-ignition engine. Energies 2021;14(14).
- [60] Ross PJ. Taguchi techniques for quality engineering: loss function, orthogonal experiments, parameter and tolerance design. New York: McGraw-Hill; 1996.
- [61] Westbrook CK, Pitz MMWJ, Kukkadapu G, Wagnon S, Zhanga K. Multi-fuel surrogate chemical kinetic mechanisms for real world applications. Phys Chem Chem Phys 2018:20:10588–606.
- [62] Wang Y, Han HS, Sohn CH. A comparative Study of chemical-kinetic mechanisms for combustion of Methane/Hydrogen/Air mixtures. International Journal of Aeronautical and Space Sciences 2024;25:519–39.
- [63] Meulemans M, Durocher A, Versailles P, Bourque G, Bergthorson JM. How well do we know thermal-NO?An investigation of NO formation in flames over a wide temperature range. Proc Combust Inst 2023;39(1):521–9.
- [64] Sun X, Jiang Y, Chen G, Jing G, Ma T. Research on thermal and fuel NOx formation mechanism of ammonia-diesel marine engines. Int J Hydrogen Energy 2025;102: 635-46
- [65] Nasim MN, Landis J, Das SK, Nawaz B, Mack JH. Reducing NOx emissions from Ammonia Combustion Through Staged Combustion. In: ASME 2024 ICE Forward Conference; 2024. San Antonio, Texas, USA.
- [66] Iavarone S, Parente A. NOx Formation in MILD combustion: potential and limitations of existing approaches in CFD. Front Mech Eng 2020;6(13).